

**EFFECT OF ANNEALING ON
MICROSTRUCTURE AND MECHANICAL
PROPERTIES OF 0.06% CARBON STEEL**

PHOUMIPHON NORDALA

UNIVERSITI SAINS MALAYSIA

2017

**EFFECT OF ANNEALING ON MICROSTRUCTURE AND MECHANICAL
PROPERTIES OF 0.06% CARBON STEEL**

by

PHOUMIPHON NORDALA

**Thesis submitted in fulfilment of the
requirements for the degree of
Doctor of Philosophy**

February 2017

DECLARATION

I hereby declare that I have conducted, completed the research work and written the thesis entitles “*Effect of Annealing on Microstructure and Mechanical Properties of 0.06% Carbon Steel*”. I also declare that it has not been previously submitted for the award of any degree of diploma or other similar title of this for any other examining body or University.

Signature :

Name of Candidate : Phoumiphon Nordala

Matrix Number : P-GD0013/13(R)

Date :

Witness by

Signature:

Main-Supervisor : Assoc. Prof. Ahmad Badri Bin Ismail

Date :

ACKNOWLEDGEMENTS

I would like to express my most sincere thanks that come deeply from my bottom of heart to all who supported my study for completing this thesis. Especially I would like to give great appreciation to my principle supervisor, Assoc. Prof. Ahmad Badri Ismail of Universiti Sains Malaysia, for his excellent scientific guidance, inspiration, and trust. Without his endless support, it is impossible for me to finish my doctoral program and this thesis. At the same time, I would like to thank deeply to my co-supervisor, Prof. Dr. Radzali Othman of Universiti Teknikal Malaysia Melaka, for his support and sincere guidance, helpful discussion. I would also like to express my sincere gratitude to my Japanese Co-supervisor Prof. Dr. Nobuhiro Tsuji of Kyoto University for his support, guidance and advice on my research. I would like to thank Assoc. Prof. Thongvanh Villayphonh of National University of Laos and Dr. Tan Boon Khoon, for their help and supports.

Special thanks and gratefully acknowledge to AUN/SEED-Net, JICA for giving me the opportunity and financial support to pursue my study. My special thanks and appreciation are also extended to AUN/SEED-Net, JICA officers for their excellent services.

I would like to express my sincerest appreciation to Dean, Deputy Dean, lecturers, all staffs and technicians of School of Materials and Mineral Resources Engineering, Universiti Sains Malaysia, for their kind assistants and supports. Without their kind cooperation, this thesis could not be completed on time.

Last but not least, I would like to express my highest gratitude to my beloved family for their love, care and support throughout the period of completing this thesis.

PHOUMIPHON NORDALA

TABLE OF CONTENTS

	Page
ACKNOWLEDGEMENTS	ii
TABLE OF CONTENTS	iii
LIST OF TABLES	vi
LIST OF FIGURES	vii
LIST OF SYMBOLS	xiv
LIST OF ABBREVIATIONS	xvi
ABSTRAK	xviii
ABSTRACT	xix
CHAPTER ONE: INTRODUCTION	
1.1 Introduction	1
1.2 Problem statement	3
1.3 Objectives	6
1.4 Scope of research	6
1.5 Outline of thesis	7
CHAPTER TWO: LITERATURE REVIEW	
2.1 Introduction	9
2.2 Steels	9
2.2.1 Low-carbon steel	13
2.3 Cold rolling	16
2.3.1 Dislocations	22
2.4 Heat treatment	24
2.4.1 Annealing	26
2.5 Iron – iron carbide (Fe – Fe ₃ C) phase diagram	28
2.6 Time, temperature, transformation (T-T-T) diagram	31
2.7 Phase transformation	32
2.7.1 Nucleation	34
2.7.2 Recovery	35
2.7.3 Recrystallization	37
2.7.4 Grain Growth	40

2.8	Microstructure of low-carbon steel	43
2.9	Transformation product	45
2.9.1	Ferrite	45
2.9.2	Pearlite	48
2.9.3	Martensite	52
2.10	Improvement mechanical properties of low-carbon steel	56

CHAPTER THREE: MATERIALS AND METHODOLOGY

3.1	Introduction	61
3.2	Materials	62
3.3	Research Methodology	62
3.4	Cold rolling	66
3.5	Materials Characterization	67
3.5.1	Optical microscopy analysis with attached image analyzer (OM-IA)	68
3.5.2	X-ray diffraction (XRD) analysis	68
3.5.3	Field emission scanning electron microscopy (FESEM) and energy dispersive X-ray (EDX) analysis	70
3.6	Mechanical test	71
3.6.1	Hardness test	71
3.6.2	Tensile test	72

CHAPTER FOUR: RESULTS AND DISCUSSION

4.1	Introduction	74
4.2	Microstructure evolution	74
4.2.1	As-received specimen	75
4.2.2	Initial microstructures	77
4.2.3	Microstructures after cold rolling AC, IWQ, and SQ specimen	84
4.2.4	Microstructures obtained after subcritical annealing temperatures	87
4.2.5	Occurrence of ultrafine grains after subcritical annealing at 500°C to 600°C	92
4.2.6	Microstructures obtained after intercritical Annealing temperatures	96
4.3	Mechanical properties	103
4.3.1	Tensile testing	103

4.3.1.1 Tensile of conventional cold rolling and subcritical annealing temperatures	103
4.3.1.2 Tensile of ultrafine ferrite grains	107
4.3.1.3 Tensile of cold rolling and intercritical annealing temperatures	113
4.3.2 Hardness testing	118
4.3.2.1 Microharness of conventional cold rolling and subcritical annealing temperatures	119
4.3.2.2 Microhardness of ultrafine ferrite grains obtained after cold rolling and subcritical annealed at temperatures ranging from 500°C to 600°C	122
4.3.2.3 Microhardness of cold rolling and intercritical annealing at various temperatures	126
4.4 X-ray diffraction results of the as-received and IWQ specimen throughout the processes.	130
4.5 Tensile strength and microhardness with subcritical annealing temperature of IWQ specimen	132
4.6 Tensile strength and microhardness with intercritical annealing temperature of IWQ specimen	134
4.7 Results comparison/ Summary	136

CHAPTER FIVE: CONCLUSIONS AND RECOMMENDATIONS FOR FUTURE RESEARCH

5.1 Conclusions	138
5.2 Recommendations for future	140

REFERENCES	141
-------------------	-----

APPENDICES

Appendix A: Percentage composition of Fe₃C

Appendix B: XRD references files

LIST OF PUBLICATIONS AND CONFERENCES

LIST OF TABLES

		Page
Table 2.1	Shows the effect of alloying elements added to steel together with the dissimilar chemical composition range used (Tisza, 2001, Davis, 2001)	11
Table 2.2	Compositions of plain low carbon steels (Rakhit, 2013)	14
Table 2.3	Mechanical characteristics of hot-rolled material and typical applications for various plain low carbon steels (Alta et al., 2012; Rakhit, 2013)	15
Table 2.4	The changing of structure during heat treatment (Hosford, 2012)	33
Table 2.5	Microstructure constituents that might occur in low-carbon steels (Brooks, 1996; Samuels, 1999; Bramfitt et al., 2001)	44
Table 3.1	Chemical composition of low-carbon steel studied (%wt)	62
Table 4.1	Volume fraction of detecting phases in the quenching specimens, measured by MangniSci Software	78
Table 4.2	Volume fraction of detecting phases in the intercritical annealing temperature, measured by MangniSci Software	99

LIST OF FIGURES

		Page
Figure 1.1	Schematic of Ford Car-2014 model, displaying the dissimilar types of materials for designing the body of the car (Mike, 2016)	2
Figure 1.2	Flowchart of research	8
Figure 2.1	Classification scheme for the various of steels (Gouda, 2014)	10
Figure 2.2	Microstructure of low-carbon steel (0.17 wt% C) F: ferrite, P: pearlite(Mazaheri et al., 2014)	16
Figure 2.3	Schematic illustration of cold rolling (Huot et al., 2012)	17
Figure 2.4	Schematic during loading and unloading cycles of stress-strain curve for (a) elastic deformation, (b) plastic deformation (Suryanarayana, 2011)	18
Figure 2.5	Stress-strain curve for low-carbon steel	19
Figure 2.6	The grain structure of low carbon steel produced by cold rolling: (a) 10%, b) 30%, (c) 60% and (d) 90% in thickness reduction (Mills et al., 1985)	20
Figure 2.7	Stress-strain curves of the sample in as-received condition compared with as-cold-rolled 93% reduction of lath martensite (Tianfu et al., 2006)	21
Figure 2.8	Transmission Electron Microscope (TEM) micrograph of 30% cold-drawn and subcritical annealed at 400°C (Hui et al., 2016)	23
Figure 2.9	Transmission Electron Microscope (TEM) micrographs for the dislocation in ferrite. Ti-free-steel without strain (a) and with 5.65% strain (b); Ti-steel without strain (c) and with 5.65% strain (d) (Tsai et al., 2017)	24
Figure 2.10	The iron – iron carbide (Fe – Fe ₃ C) phase diagram. α , δ = Ferrite; γ = Austenite; L = Liquid; Fe ₃ C = Cementite (Grote et al., 2009)	29
Figure 2.11	The complete T-T-T diagram for an iron-carbon alloy of eutectoid composition (Zhang et al., 2011)	32

Figure 2.12	The demonstration of (a) occurrence of nucleation, (b) increasing of nucleation size (Rollett et al., 2004)	35
Figure 2.13	Schematics displaying the cell structures dislocation tangles change through cell structures to subgrains during recovery. (a) dislocation defects, (b) rearrangement of dislocations, (b) forming of cellular structure, (c) forming of subgrain boundaries (Verlinden et al., 2007)	36
Figure 2.14	Microstructure of TWIP steel after 50% cold-rolling; (a) and (b) recovery annealing, (c) partial recrystallization- observed by EBSD mappings (Haase et al., 2016)	37
Figure 2.15	Schematic of recrystallization taking place during the annealing of strain hardened material. (a) work hardened grains, (b) subgrains and recrystallization nuclei, (b) recrystallized grains (Saki et al., 2014)	38
Figure 2.16	Schematic of strength and ductility of a metal as a function of the percentage of cold-work and time of annealing (Anusavice et al., 2014)	39
Figure 2.17	Electron Backscatter Diffraction (EBSD) measured recrystallization (yellow colour) of specimens heating at 50°C/s at different temperatures: (a) 690°C, (b) 730°C (Liu et al., 2016)	40
Figure 2.18	Large grain expense of their neighbours and smaller grains shrink (Hosford, 2012)	41
Figure 2.19	The orientation image map (OIM) to rolling reduction (RD) of the cold-rolled high silicon electrical steel sheet with annealed at 1100°C (a), 1200°C (b), and 1300°C (c) for 1 hour (Pan et al., 2016)	42
Figure 2.20	Grain and the nature of the grain boundaries of α -ferrite crystal structure (Verhoeven, 2007)	46
Figure 2.21	Microstructure of a fully ferritic of ultralow carbon steel, 300x (Bramfitt, 1998)	47
Figure 2.22	Austenite to pearlite colony transformation, the schematic representation of alternate layers of cementite and ferrite formation (Suryanarayana, 2011)	49
Figure 2.23	Schematic reaction curves for (A) isothermal formation of pearlite, (B) T-T-T diagram obtained from reaction curves (Abbaschian et al., 2009)	50

Figure 2.24	Microstructure of (a) coarse pearlite, and (b) fine pearlite in 1075 (Levy, 1981)	50
Figure 2.25	The formation of the pearlite microstructure on chilling a 0.77% carbon steel below eutectoid temperature (727°C) on the iron-carbon phase diagram. α : ferrite, γ : austenite, Cm: cementite (Fe_3C), A_1 : eutectoid temperature, A_3 : the boundary between γ and the two-phase field containing of ($\alpha + \gamma$), A_{cm} : the boundary between γ and the two-phase field containing of (Cm + γ) (Verhoeven, 2007)	51
Figure 2.26	Random process of martensite phase (a) Martensite formation, (b) growth of martensite with decreasing cooling below martensite start (M_s) temperature. γ : austenite phase, α' : martensitic phase (Porter et al., 1992)	52
Figure 2.27	Effect of weight percentage carbon content on the martensite start (M_s) temperature in steels (Bramfitt, 1998)	53
Figure 2.28	Microstructure of (a) lath martensite in the 0.2C-2Mn steel (Morito et al., 2005), (b) plate martensite in the 1.2C-0.3Mn steel (Stormvinter et al., 2012)	54
Figure 2.29	The hardness of martensite, pearlite and spheroidized cementite structures steels as a function of their carbon concentration (Abbaschian et al., 2009)	55
Figure 3.1	Flow chart of research activities	61
Figure 3.2	Schematic thermomechanical processes employed to develop different initial microstructures by air-cooling (AC)	64
Figure 3.3	Schematic thermomechanical processes employed to develop different initial microstructures by ice-water quenching (IWQ)	65
Figure 3.4	Schematic thermomechanical processes employed to develop different initial microstructures by step-quenching (SQ)	65
Figure 3.5	Rolling machine, roller diameter of 80 mm	67
Figure 3.6	Surface of the specimen to be examined	67
Figure 3.7	Illustration of Bragg's Law (Mahato et al., 2009)	69
Figure 3.8	Schematic of indentation mark in Vickers hardness measurement	72
Figure 3.9	Dimension of the tensile specimen	73

Figure 4.1	Optical microstructure of the as-received specimen, observed at a magnification of 500x. Ferrite = F, Pearlite = P.	76
Figure 4.2	EDX results of ferrite = F (a), and pearlite = P (b) in the as-received microstructure	76
Figure 4.3	Ferrite grain size distribution of as-received specimen	77
Figure 4.4	Microstructure of specimens after quenching: (a) AC, (b) IWQ, and (c) SQ, observed at a magnification of 500x. Ferrite = F, Pearlite = P, Martensite = M	80
Figure 4.5	FESEM and EDX results of (a) pearlite in AC, (b) martensite in IWQ, and (c) martensite in SQ. Ferrite = F, Pearlite = P, Martensite = M	83
Figure 4.6	Ferrite grain size of specimens after quenching: (a) AC, (b) IWQ, and (c) SQ	84
Figure 4.7	Microstructure of the 75% cold-rolled specimen: (a) AC, (b) IWQ, and (c) SQ. Observed at a magnification of 500x	86
Figure 4.8	The wavy ferrite bent along the martensite after 75% cold rolled specimen: (a) IWQ, and (b) SQ. M = martensite, F = ferrite. Observed at a magnification of 1000x.	86
Figure 4.9	Microstructure of 75% cold-rolled AC, IWQ, and SQ specimens and then annealed at various temperatures: (a) AC 200°C, (b) IWQ 200°C, (c) SQ 200°C; (d) AC 300°C, (e) IWQ 300°C, (f) SQ 300°C; (g) AC 400°C, (h) IWQ 400°C, (i) SQ 400°C; (j) AC 500°C, (k) IWQ 500°C, (l) SQ 500°C; (m) AC 600°C, (n) IWQ 600°C, (o) SQ 600°C; (p) AC 700°C, (q) IWQ 700°C, (r) SQ 700°C	89
Figure 4.10	Microstructures of AC, IWQ, and SQ specimens after 75% cold-rolled and annealed at 500°C - 600°C for 30 min: (a) AC 500°C, (b) IWQ 500°C, (c) SQ 500°C; (d) AC 525°C, (e) IWQ 525°C, (f) SQ 525°C; (g) AC 550°C, (h) IWQ 550°C, (i) SQ 550°C; (j) AC 575°C, (k) IWQ 575°C, (l) SQ 575°C; (m) AC 600°C, (n) IWQ 600°C, (o) SQ 600°C. Observed under FESEM, Magnification of 10KX	94
Figure 4.11	Optical microstructures of AC, IWQ, and SQ produced by 75% cold-rolled and intercritical annealed at various temperatures. Observed from TD with magnification of 500x under OM-IA	98

Figure 4.12	Schematic of the microstructure evolution during thermomechanical process. α = ferrite, γ = austenite, Fe_3C = cementite.	99
Figure 4.13	FESEM and EDX results of the IWQ specimen after 75% cold-rolled and intercritical annealed at 800°C for 10 min before ice-water quenching. (a) observed with magnification of 1000x, (b) observed with magnification of 5000x. M = martensite, F = ferrite	101
Figure 4.14	Stress-strain curves of the as-received, AC, cold-rolled, and annealed at various temperatures for 30 min	105
Figure 4.15	Stress-strain curves of the as-received, IWQ, cold-rolled, and annealed at various temperatures for 30 min	106
Figure 4.16	Stress-strain curves of the as-received, SQ, cold-rolled, and annealed at various temperatures for 30 min	106
Figure 4.17	Stress-strain curves of the as-received and annealed specimens after 75% cold-rolled AC at various temperatures for 30 min.	108
Figure 4.18	Stress-strain curves of the as-received and annealed specimens after 75% cold-rolled IWQ at various temperatures for 30 min	108
Figure 4.19	Stress-strain curves of the as-received and annealed specimens after 75% cold-rolled SQ at various temperatures for 30 min	109
Figure 4.20	Stress-strain curves of the as-received and subcritical annealed specimens after 75% cold-rolled AC, IWQ, and SQ at 525°C for 30 min	110
Figure 4.21	Stress-strain curves of the as-received, AC, 75% cold-rolled, and annealed specimens at various temperatures for 10 min before ice-water quenching.	114
Figure 4.22	Stress-strain curves of the as-received, IWQ, 75% cold-rolled, and annealed specimens at various temperatures for 10 min before ice-water quenching	116
Figure 4.23	Stress-strain curves of the as-received, SQ, 75% cold-rolled and annealed specimens at various temperatures for 10 min before ice-water quenching	116
Figure 4.24	Stress-strain curves of the as-received and annealed specimens after 75% cold-rolled AC, IWQ, and SQ at 800°C for 10 min before ice-water quenching	117
Figure 4.25	Microhardness of the as-received, AC, cold-rolled, and subcritical annealed at various temperatures for 30 min	121

Figure 4.26	Microhardness of the as-received, IWQ, cold-rolled, and subcritical annealed at various temperatures for 30 min	121
Figure 4.27	Microhardness of the as-received, SQ, cold-rolled, and subcritical annealed at various temperatures for 30 min	122
Figure 4.28	Microhardness of the as-received and AC specimens after 75% cold-rolled and subcritical annealed at various temperatures ranging from 500°C to 600°C for 30 min.	124
Figure 4.29	Microhardness of the as-received and IWQ specimens after 75% cold-rolled and subcritical annealed at various temperatures ranging from 500°C to 600°C for 30 min	124
Figure 4.30	Microhardness of the as-received and SQ specimens after 75% cold-rolled and subcritical annealed at various temperatures ranging from 500°C to 600°C for 30 min	125
Figure 4.31	Microhardness of the as-received and AC, IWQ, and SQ specimens after 75% cold-rolled and subcritical annealed at 525°C for 30 min	126
Figure 4.32	Microhardness of the as-received, AC, after 75% cold-rolled and intercritical annealed at various temperatures for 10 min followed by ice-water quenching	128
Figure 4.33	Microhardness of the as-received, IWQ, 75% cold-rolled and intercritical annealed at various temperatures for 10 min followed by ice-water quenching	128
Figure 4.34	Microhardness of the as-received, SQ, 75% cold-rolled and intercritical annealed at various temperatures for 10 min followed by ice-water quenching	129
Figure 4.35	Microhardness of the as-received and intercritical annealed specimens after 75% cold-rolled AC, IWQ, and SQ at 800°C for 10 min followed by ice-water quenching	130
Figure 4.36	X-ray diffraction patterns for the as-received, IWQ, and IWQ specimen cold-rolled at 75%, subcritical annealed at 525°C and intercritical annealed at 800°C.	132
Figure 4.37	Variation in the tensile strength with subcritical annealing temperature of IWQ specimen	133
Figure 4.38	Variation in the microhardness with subcritical annealing temperature of IWQ specimen	134
Figure 4.39	Variation in the tensile strength with intercritical annealing temperature of IWQ specimen	135

Figure 4.40	Variation in the microhardness with intercritical annealing temperature of IWQ specimen	135
Figure 4.41	Stress-strain curves of current study compared to previous studies. UFG: ultrafine grain, DP: dual-phase ferrite-martensite, Referenced (i) studied by (Wang et al., 2005), Referenced (ii) studied by (Azizi-Alizamini et al., 2007)	137

LIST OF SYMBOLS

%	Percentage
%C	Percentage of Carbon
%wt	Weight Percentage
%EL	Percentage of Elongation
F	Ferrite
M	Martensite
P	Pearlite
>	More Than
<	Less Than
~	Approximately/ About
°C	Degree Celsius
K	Kelvin
g	Gram
Min	Minute
MPa	Megapascal
mm	Milimeter
μm	Micrometer
Nano	Nanometer
Fe ₃ C	Cementite/Carbide
γ	Austenite (gamma)
α	Ferrite (alpha)
λ	Wavelength of the Rays
θ	Angle between the Incident Rays and the Surface of the Crystal

D	Spacing between the Layers of Atoms
T_m	Melting Temperature
M_s	Martensite Start
M_f	Martensite Finish
ϵ_{eq}	Equivalent Strain
n	Total Number of Rolling Passes
r	Reduction at Each Pass

LIST OF ABBREVIATIONS

DP	Dual Phase
UFG	Ultrafine Grain
SPD	Severe Plastic Deformation
ECAP	Equal Channel Angular Pressing
ARB	Accumulative Roll-Bonding
HPT	High Pressure Torsion
MDF	Multidirectional forging
ASTM	American Society for Testing and Materials
AISI	American Iron and Steel Institute
SAE	Society of Automotive Engineers
FCC	Face Centered Cubic
BCC	Body Centered Cubic
BCT	Body Cetered Tetragonal
IT	Isothermal Transformation
TWIP	Twinning-Induced Plasticity
AC	Air-Cooling
IWQ	Ice-Water Quenching
SQ	Step-Quenching
CR	Cold Rolling
OM-IA	Optical Microscopy Analysis with attached Image Analyzer
XRD	X-ray Diffraction
FESEM	Field Emission Scanning Electron Microscopy
EDX	Energy Dispersive X-ray

HV	Vickers Hardness
RD	Rolling Direction
TD	Transverse Direction

KESAN PENYEPUHLINDAPAN KE ATAS MIKROSTRUKTUR DAN SIFAT-SIFAT MEKANIKAL BAGI KELULI KARBON 0.06%

ABSTRAK

Kajian ini bertujuan untuk mengkaji mikrostruktur dan sifat mekanik keluli rendah karbon (0.06% C) terhadap beberapa proses rawatan haba dan kerja sejuk. Proses ini bermula dengan tiga rawatan haba yang berbeza; Penyejukan Udara (AC), Pelindapkejutan Air dan Ais (IWQ), dan Penyepuhlindapan Bertingkat (SQ) sebelum 75% pengelekan-sejuk. Semua spesimen tergelek-sejuk disepuhlindap pada suhu sub-genting dan inter-kritikal. Keputusan menunjukkan bahawa IWQ adalah kaedah terbaik untuk memulakan mikrostruktur awal berbanding dengan kaedah AC dan SQ. Suhu penyepuhlindapan optimum sub-genting adalah pada 525°C. Pada suhu ini (525°C), butiran ferit ultra-halus diperolehi (~ 500 nm). Kekuatan tegangan dan mikro-kekerasan adalah lebih tinggi daripada keadaan diterima kira-kira 89% dan 79% masing-masing. Tambahan pula, didapati bahawa suhu penyepuhlindapan inter-kritikal yang optimum adalah pada 800°C. Pada suhu ini (800°C), kombinasi ferit dan martensit yang terbaik terbentuk. Kekuatan tegangan dan mikro-kekerasan adalah lebih tinggi daripada spesimen yang diterima lebihkurang 81% dan 104%, masing-masing.

EFFECT OF ANNEALING ON MICROSTRUCTURE AND MECHANICAL PROPERTIES OF 0.06% CARBON STEEL

ABSTRACT

The present study is aimed to examine the microstructure and mechanical properties of low-carbon (0.06% C) steel against several heat treatment and cold worked processes. The process was started with three different heat treatments; Air Cooling (AC), Ice-Water Quenching (IWQ), and Step Quenching (SQ) prior 75% cold rolling. All cold-rolled specimens were subcritical and intercritical annealing. The results show that the IWQ is the best method to start initial microstructure compared to AC and SQ method. The optimum of subcritical annealing temperature is at 525°C. At this temperature (525°C), ultrafine ferrite grains are obtained (~ 500 nm). Tensile strength and microhardness are higher than as-received condition about 89% and 79%, respectively. Furthermore, it was found that the optimum intercritical annealing temperature is at 800°C. At this temperature (800°C), a good combination of ferrite and martensite are formed. The tensile strength and microhardness are higher than the as-received specimen about 81% and 104%, respectively.

CHAPTER ONE

INTRODUCTION

1.1 Introduction

In general terms, iron and steel are often confusing. Iron is a chemical element (atomic number 26 on the periodic table). The symbol of chemical 'Fe' is from the Latin word for iron, Ferrum. The word steel is used to describe almost all alloy of iron and it is often mentioned that steel is an alloy of iron and other elements, primarily carbon (Hosford, 2012). The basic material in human development is steel. An adequate quantity of quality steel materials is essential for the realization of industrial development of countries all over the world and for supplying conditions for the modern lifestyle of humanity. Steel is a necessary component of all machinery used for the manufacture of all our goods (Weng, 2009). The study of steels is essential because of the steel represents by far the most extensively-utilized metallic materials, basically due to steel can be manufactured cheaply in large quantities to accurate specifications (Bhadeshia et al., 2011). On the other hand, the wide range of desirable properties which can be managed easily by altering the elemental composition and processing.

The increasing rapidly of motor vehicles worldwide and the associated environmental impact, lightweighting automobile has become an urgent global initiative. In order to provide automobile market requirements such as lightweight materials to improve vehicles with high fuel efficient. The automobile industry has developed steels which are advanced high strength steels (AHSS) together with dual-phase (DP) steels. These steels display both high strength and excellent formability

with weight reduction (Cornette et al., 2001; Shaw et al., 2001). The most common steels used in the automobile industry are mild steels, which are low-carbon steels due to it is cheap and excellent deep draw ability.

Figure 1.1 is a schematic of the Ford Car-2014 model, displaying the dissimilar types of materials that used for designing the body of the car. It can be seen that the bulk of the car body consists of dual-phase steels and mild steels which are low-carbon steels are predominantly used. Hence, the present study is attempting to investigate a plain low-carbon steel.

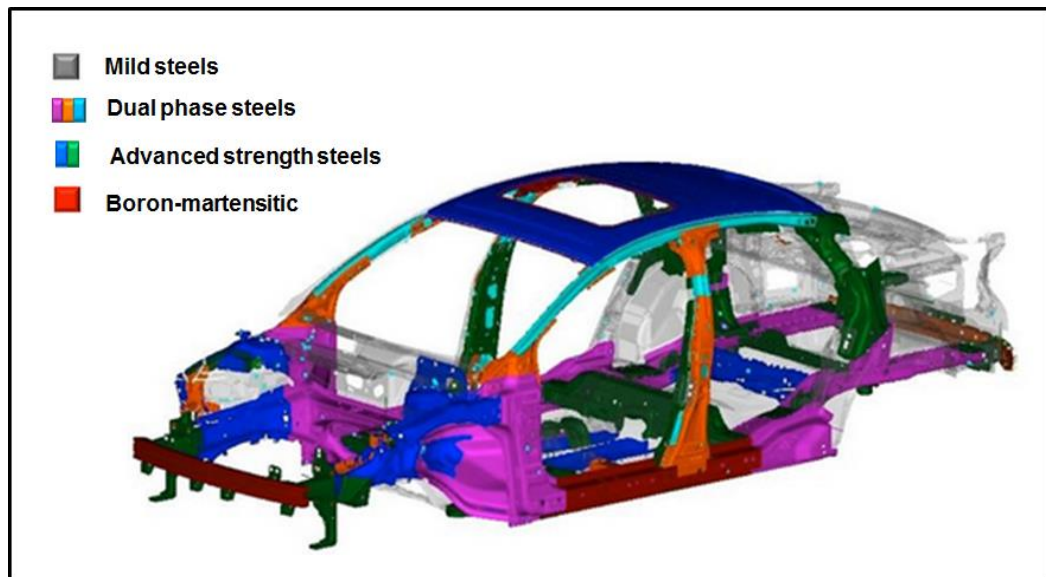


Figure 1.1 Schematic of Ford Car-2014 model, displaying the dissimilar types of materials for designing the body of the car (Mike, 2016).

1.2 Problem statement

Low-carbon steel is known as low mechanical properties and they have very limited applications compare to other higher mechanical properties steels. Many research groups have investigated various innovative methods to improve the strength of low-carbon steel. The methods include Severe Plastic Deformation (SPD) processes such as Equal Channel Angular Pressing (ECAP) (Nejnoto et al., 1998; Horita et al., 2000; Valiev et al., 2006), Accumulative Roll-Bonding (ARB) (Saito et al., 1998; Tsuji et al., 2002b), and High Pressure Torsion (HPT) (Valiev, 1997; Huang et al., 2003). By using these methods, ultrafine grains steel (grains size smaller than 1 μm) with superior mechanical properties (Tsuji et al., 2002b; Valiev et al., 2006) can be achieved.

Besides the SPD processes have been reported by other researchers as well. Fu et al., (2007) had improved the strength of low-carbon (0.10-0.25% C) steels by adding elements such as Titanium (Ti) and Cerium rare earth (Ce) into steels. They had found that tensile strength improved up to about 36% compared with the sample without addition of Ti and Ce. In addition, Li et al., (2014a) lately enhanced mechanical properties of low-carbon (0.091% C) steel by adding Manganese (Mn) and Titanium (Ti) alloy elements. The results showed a yield strength of 920 MPa with elongation about 10%.

Although all these methods have played a big role in improving mechanical properties of low-carbon steels, but they also show drawbacks as following:

- (i) SPD processes are difficult for bulk production, particularly in producing large dimension of UFG steel with appropriate strength